JGR Solid Earth

RESEARCH ARTICLE
10.1029/2023JB028546

A Global Marine Sediment Compilation and a Cerium Anomaly Perspective on Metasomatized Mantle Sources for REE-Mineralized Carbonatites

Michael Anenburg[1] and **Yan Liu**[2]

[1]Research School of Earth Sciences, Australian National University, Canberra, ACT, Australia, [2]SinoProbe Laboratory, Institute of Geology, Chinese Academy of Geological Sciences, Beijing, China

Key Points:

- Subducted REE-rich sediments with negative Ce anomalies are thought to supply carbonatites with their REE
- Carbonatites have no statistically significant negative Ce anomaly
- Recycling of particularly REE-rich marine sediments not required for mineralization

Correspondence to:
M. Anenburg,
michael.anenburg@anu.edu.au

Citation:
Anenburg, M., & Liu, Y. (2024). A global marine sediment compilation and a cerium anomaly perspective on metasomatized mantle sources for REE-mineralized carbonatites. *Journal of Geophysical Research: Solid Earth*, *129*, e2023JB028546. https://doi.org/10.1029/2023JB028546

Received 13 DEC 2023
Accepted 21 MAY 2024

Author Contributions:
Conceptualization: Michael Anenburg
Data curation: Michael Anenburg, Yan Liu
Funding acquisition: Yan Liu
Investigation: Michael Anenburg
Methodology: Michael Anenburg
Project administration: Yan Liu
Resources: Yan Liu
Software: Michael Anenburg
Visualization: Michael Anenburg
Writing – review & editing: Michael Anenburg, Yan Liu

Abstract Rare earth elements (REE) are vital for powerful permanent magnets used in electric motors and wind turbines. These elements are chiefly sourced from carbonatites and their weathering products. The economic attractiveness of carbonatites is explained by the 10,000-fold enrichment of REE in their mineralized portions relative to the average continental crust. Carbonatites form from mantle-derived melts, but the ultimate origin of their REE is not completely clear. One widely cited model invokes subduction of marine sediments which accumulate REE-rich material, priming the mantle to produce REE-rich carbonatite melts which subsequently form deposits in the upper crust. Here we examine a global marine sediment compilation, revealing a wide variety in REE abundances and patterns. We use the sensitive lambda method that separates REE pattern curvature from redox-related element anomalies to examine both marine sediments and presumably derived carbonatite rocks. We find that the most REE-rich marine sediments are characterized by strongly negative Ce anomalies, which if recycled via subduction, mineralized carbonatites are expected to inherit. In contrast, we find that mineralized carbonatite rocks do not contain Ce anomalies. This indicates that the REE from the most REE-rich marine sediments are not recycled into carbonatite deposits, and a different REE source is needed to explain carbonatite fertilities. We also find evidence that raises questions on whether any sediment-derived REE are present in carbonatite deposits to a significant amount. We suggest that a REE-rich source may not be required and REE enrichment occurs primarily during crustal magmatic differentiation.

Plain Language Summary Rare earth elements (REE) such as neodymium are important components of permanent magnets used in energy generation technologies including wind power turbines and electric motors. These metals are extracted from carbonatite rocks, but how the REE got to carbonatites in the first place is contentious. The seafloor contains accumulations of exceptionally REE-rich sediments, and a popular model proposes that these REE are recycled to the mantle during subduction. Once melting occurs in the mantle, these same REE are suggested to be transported in the carbonatite melts and eventually reach the upper crust where they contribute to economic mineralization. However, the REE-rich sediments contain a ubiquitous chemical signature in the form of a redox-sensitive negative cerium anomaly. We show that the anomaly does not occur in carbonatite rocks, with the implication that recycled REE-rich sediments cannot necessarily be the source for carbonatite-related ore deposits.

1. Introduction

Carbonatites are igneous rocks composed primarily of the carbonate minerals calcite and dolomite (Yaxley et al., 2022). They are the largest source for REE (the rare earth elements La to Lu), metals crucial for emerging zero-emission energy generation technologies such as wind turbines and electric vehicle motors (Simandl & Paradis, 2018). A still open question concerns the provenance of the REE: where are the carbonatite-hosted REE coming from? There is widespread agreement that REE are sourced from the mantle, but how the REE got there in the first place is still uncertain. Different hypotheses provide different answers, and depend on which deposit is studied. Furthermore, different isotopic systems (e.g., Sr–Nd–Hf–B–Pb–C–S) may lead to contrasting answers, because not all chemical components necessarily derive from the same source. A depleted mantle origin has been proposed for deposits such as Fen in Norway and Chilwa Island in Malawi using Sr–Nd isotopes (Andersen, 1987; Simonetti & Bell, 1994). Alternatively, other deposits such as Catalão (Brazil), Yangibana (Australia), and Maoniuping (China) have been suggested to derive from a metasomatized or enriched mantle using Sr–Nd–Hf isotopes (Guarino et al., 2017; Slezak & Spandler, 2019; Weng et al., 2021). Many carbonatites lie on an array

or continuum between the depleted mantle and the various enriched mantle components such as EM1 and EM2 (Bell & Tilton, 2001; Nelson et al., 1988; Smith et al., 2016; Yaxley et al., 2022). These enriched mantle components are particularly interesting because they potentially form by recycling of sediments or sediment-derived fluids back into the mantle, or alternatively by crustal assimilation of depleted mantle melts (White, 2015). These sediments sample the REE composition of the upper continental crust, which is on average enriched in REE—and specifically the lighter REE (LREE)—relative to the mantle due to their incompatible behavior during mantle melting and magmatic differentiation processes (with enrichment factors between about 10 and 100, Plank, 2014). Following this reasoning, Smith et al. (2016) suggested that carbonatites derived from enriched mantle components host larger amounts of contained REE. However, a counterexample is Mount Weld (Western Australia), one of the largest carbonatite-hosted REE deposits on Earth, yet it exhibits no enriched mantle component (Chandler et al., 2024; Nelson et al., 1988). Evidently, an enriched mantle component is not a crucial factor to the formation of a major REE deposit. The mantle source may not even be important, with Anenburg et al. (2021) suggesting that igneous differentiation processes occurring within the crust lead to mineralization (albeit not necessarily economic), regardless of how and where the carbonatite melt initially formed.

REE patterns of subducting sediments typically reflect the upper continental crust from which they derive, as summarized in the global subducting sediment (GLOSS and GLOSS-II) models (Plank, 2014; Plank & Langmuir, 1998). These sediments are enriched in the LREE, similar to the REE budget of carbonatites (albeit to a lesser degree). Despite this observed LREE-enrichment in subducting sediments, the average subducting sediment is not particularly REE-rich (e.g., La, Ce, and Nd only reach a few tens of ppm, Plank, 2014) and the process by which such a sediment might lead to REE mineralization is unclear. A model first developed by Hou et al. (2015) attempted to address this issue. Using the example of carbonatite-associated REE deposits from the Cenozoic Mianning-Dechang belt in China, Hou et al. (2015) proposed that the exceptional REE enrichment of these deposits did not result from a mantle that was enriched by just average subducting marine sediments (such as GLOSS). Instead, they invoke subduction of particularly "REE-rich" sediments, motivated by the discovery of localized regions on the ocean floor containing highly REE-rich marine sediments with up to thousands of ppm of ΣREE (Y. Deng, Guo, et al., 2022; Kato et al., 2011; Mimura et al., 2019; Takaya et al., 2018; Wang et al., 2017, 2021; Yasukawa et al., 2014, 2020). This process was suggested by Hou et al. (2015) to feed an enriched REE material, as well as abundant carbonate, back into the mantle such that when carbonatites form they are REE-rich at source and more conducive for economic concentration upon reaching the upper crust (Hou et al., 2015). This model has proven popular (J. Deng, Wang, et al., 2022; Hou et al., 2023; N.-B. Li et al., 2022; Weng et al., 2021; L.-Q. Yang et al., 2022), and adopted for many deposits elsewhere in the world (Ding et al., 2022; Gao et al., 2021; Goodenough et al., 2021; Grabarczyk et al., 2022; Hussain et al., 2020; X.-C. Li, Zhou, et al., 2023; Nedosekova et al., 2021; Xue et al., 2018; Zhao et al., 2021).

Although the Hou et al. (2015) model is attractive, it lacks a thorough assessment of REE in the subducted material. There is no one "REE-rich" sediment type or composition. To a first order approximation, the two REE-rich sediment types are (a) Mn-rich nodules and crusts (e.g., H. Zhang et al., 2023), and (b) phosphate-rich sediments (e.g., Ren et al., 2022). REE patterns of certain marine sediment types commonly contain Ce anomalies arising from the higher oxidation state of Earth's surface compared to its interior. Cerium occurs either as Ce^{3+}, the common valence in most deep Earth and magmatic conditions, or as Ce^{4+}, common in surface and marine conditions in which atmospheric oxygen is encountered. Trivalent Ce behaves in line with all other REE^{3+}, and follows the typically smooth trend in chondrite-normalized REE patterns. In contrast, tetravalent Ce behaves like other smaller highly charged cations (also known as the high field strength elements—HFSE) such as Zr^{4+}, Th^{4+}, Nb^{5+}, and the heaviest REE like Yb^{3+} and Lu^{3+} (Burnham & Berry, 2014). Marine sediments are sensitive to atmospheric oxygen levels (K. Zhang & Shields, 2022). Generally, Mn-rich nodules are Ce-enriched owing to the greater compatibility of Ce^{4+} in these oxide minerals, whereas phosphate-rich sediments are depleted in Ce (J. Li, Shi, et al., 2023; Liao et al., 2024; Ren et al., 2022; Yu et al., 2021; H. Zhang et al., 2023). These two effects largely cancel each other out and are diluted by the presumably more abundant non-anomalous sediments, leading to an average sediment with a negligible—potentially not statistically significant—negative Ce anomaly (i.e., GLOSS) (Plank, 2014; Plank & Langmuir, 1998). Nonetheless, the heterogenous spatial distribution of these REE-rich regions would likely result in localized domains of Ce-anomalous material subducted into the mantle. If carbonatite-hosted REE are specifically sourced from recycled REE-rich marine sediments, rather than average marine sediments, then these selfsame Ce anomalies are expected in carbonatite-hosted deposits.

Here, we compare a large global data set of REE patterns and Ce anomalies in modern marine sediments, and a diverse set of bulk rocks from Mianning-Dechang in China to quantify the role of marine sediment contribution to the REE budget of carbonatite deposits. We demonstrate a novel and sensitive method for examining Ce anomalies within the context of a complete REE pattern. We also examine three other Phanerozoic carbonatites to confirm that our model is globally generalizable beyond the Mianning-Dechang belt.

2. Materials and Methods

Representative samples from four Mianning-Dechang localities (Maoniuping, Muluozhai, Lizhuang, and Dalucao) were collected for commercial bulk rock analysis at ALS Global. REE were mostly measured by solution inductively coupled plasma mass spectrometry (ICP-MS), using the following isotopes: ^{139}La, ^{140}Ce, ^{141}Pr, ^{143}Nd, ^{147}Sm, ^{151}Eu, ^{159}Tb, ^{160}Gd, ^{163}Dy, ^{165}Ho, ^{167}Er, ^{169}Tm, ^{172}Yb, and ^{175}Lu. Some strongly REE-rich samples contained more LREE than could be measured by ICP-MS, and were measured by X-ray fluorescence (XRF) instead. Sample description and details on the process by which we merged and normalized both data sets are available in Supporting Information in https://doi.org/10.6084/m9.figshare.22097921.

We obtained a compilation containing ~6,000 REE analyses of modern marine sediments (Ren et al., 2021). The compilation includes data from the Atlantic, Pacific, and Indian oceans, and typically includes the top few of meters to tens of meters below the sea floor (Y. Deng et al., 2018; Kato et al., 2011; Menendez et al., 2017; Mimura et al., 2019; Ren, He, Yao, et al., 2017; Ren, He, Zhu, et al., 2017; Ren et al., 2015; Tanaka et al., 2020; Yasukawa et al., 2016; X. Zhang et al., 2017). These studies used bulk methods to provide information on the entire sediment composition, often a combination of XRF for major and minor elements, and ICP-MS for the REE. Detection limits are variable across these studies, but are typically 0.1 ppm. Only 18 entries did not include data for the whole REE series, with the missing elements being mostly Tm and Lu. There was no attempt to separate REE contributions from specific sediment fractions, such as clay, carbonate, phosphate, or nodules.

REE patterns from the previously compiled marine sediment data (Ren et al., 2021) and the newly acquired Mianning-Dechang rock samples were analyzed using the lambda method via the online BLambdaR application (Anenburg & Williams, 2022). This method allows deconvolution of various curvature components of patterns into independent coefficients (Anenburg & Williams, 2022; O'Neill, 2016). The coefficients represent the average normalized REE contents (λ_0), the linear slope (λ_1), the quadratic curvature (λ_2), sinusoidality (λ_3), and a higher order "W"-shape (λ_4). A linear combination of all coefficients multiplied by the shape polynomials results in a full REE pattern represented as a smooth mathematical function instead of an empirical line connecting individual REE data points (Anenburg & Williams, 2022). An instructive example of these coefficients is given in Figure 1. The lambda method considers each REE pattern as a whole, making it insensitive to uncertainties on individual elements because the polynomial fit typically smoothes out single-element noise arising from analytical uncertainty. This is particularly important for odd atomic number elements in the sub-ppm range because their analytical precision (often to 0.1 ppm) is not sufficient for a smooth line based on linear interpolation alone. The lambda method has an additional benefit of reducing REE patterns from lines to points, facilitating plotting and evaluation of large data sets and their analysis (O'Neill, 2016). The traditional method for dimension reduction of REE patterns is the calculation of normalized element ratios. However, these ratios are not independent of shape —$[La/Yb]_{CN}$, for instance, is nominally designed to capture the linear slope, but it is influenced by higher order curvatures, as well as errors in individual elemental analysis (Anenburg, 2020). In contrast, the linear slope coefficient (λ_1) is mostly immune to these hurdles. The method allows accurate Ce anomaly determination as it is quantified by the deviation of Ce from a curved polynomial fit to a normalized REE pattern (Anenburg, 2020), an improvement over traditional interpolation methods of Ce-anomaly determination, often calculated as $Ce/Ce* = Ce/\sqrt{La^2 \times Pr^2}$ (Barrat et al., 2023; K. Zhang & Shields, 2022). Furthermore, as the method outputs this deviation for all 14 REE, it is possible to compare any observed Ce anomaly to apparent anomalies in other non-redox-sensitive elements. This provides an additional check on whether the Ce anomaly is true, or whether it is within the range of other spurious anomalies that emerge in naturally noisy data sets. Given the prominent Ce anomalies in most patterns (Figure 2a), lambda coefficients were calculated considering Ce as anomalous to exclude it from the polynomial fitting, using the relevant BLambdaR setting. Europium is easily fractionated in crustal magmatic differentiation processes, and anomalies can often form even in mild surface weathering. Since we are seeking a pristine mantle signature, Eu anomalies are excluded from this analysis.

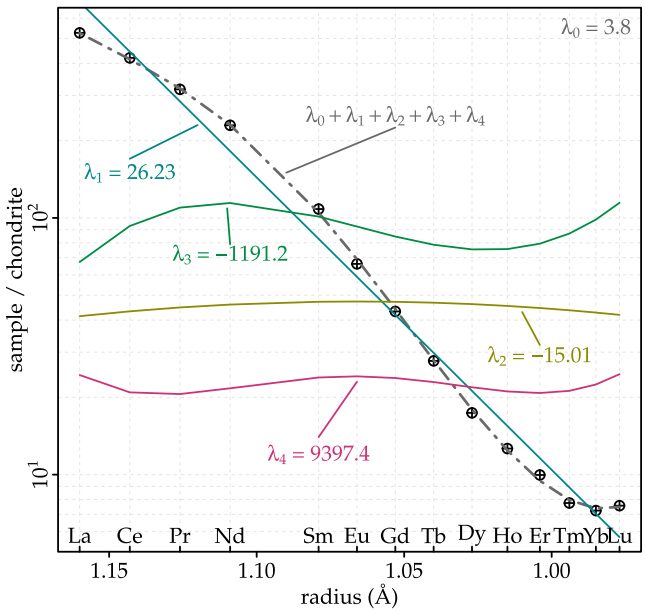

Figure 1. Lambda coefficients derived from REE data (black crosses) of a syenite from Lizhuang. Each lambda coefficient represents a different shape (colored lines). Their linear combination results in the polynomial fit (dashed line), which is almost indistinguishable from the measured data. This demonstrates the use of lambda coefficients instead of individual REE to represent REE patterns. The vertical position of each shape is arbitrary and chosen to avoid overplotting. The actual vertical position is determined by λ_0. Strictly speaking, each line is determined by lambda coefficients multiplied by orthogonal functions (i.e., $\lambda_n \times f_n^{\text{orth}}$), but here functions have been omitted for simplicity (for more details, see Anenburg & Williams, 2022; O'Neill, 2016).

3. Results

3.1. Marine Sediments

Rare earth element patterns representing more than 150 ppm of total REE are plotted in Figure 2a. This includes 3,670 out of 6,084 analyses, or about 60.3% of the total data. Patterns of analyses containing less than 150 ppm are often noisy with meaningless individual REE measurements, specifically for odd atomic number elements. Most marine sediments have a negative Ce anomaly, especially patterns that represent the REE-richest sediments (Figure 2a). A minority of patterns contain a positive Ce anomaly, particularly at the mid-range of sediment ΣREE contents (note that Figure 2a does not show the most REE-poor sediments). There is no peak or overrepresentation of non-anomalous sediments (Ce/Ce* ≈ 1). Instead, non-anomalous samples form a part of the continuum between positive and negative Ce-anomalous sediments (Figure 2b).

The vast quantity of patterns results in substantial overplotting, justifying the use of the lambda method, which effectively reduces lines (i.e., REE patterns) to points in lambda space (Figures 2b–2d). As we are particularly interested in REE abundances, we plot total REE abundances (ΣREE) against λ_0, the polynomial coefficient that represents the average REE pattern height as a proxy for REE abundance (Figure 2b). There is an excellent correlation between the two, as expected. However, the middle part splits into two parallel trends, which can be readily explained by the presence of Ce anomalies. Cerium is the most abundant out of all REE, and any deviation in its concentrations can markedly shift ΣREE to higher or lower values. Figure 2c demonstrates this better, expanding the squashed triangular shape observed in Figure 2b to fill the whole plotting region in Figure 2c. This way, the triangular shape is not obscured by the more dominant linear correlation between ΣREE and λ_0. Our use of λ_0 thus provides a better estimate of overall REE abundances in the database, as it is not biased by the disproportionate influence of anomalies in a single element (Ce) on ΣREE values. The reason for the roughly triangular distribution is curious as it indicates three endmembers that primarily mix with one other endmember at a time, rather than a mixture of all three. The reasons are unknown and beyond the scope of this study.

A comparison of GLOSS, GLOSS-II (green in Figure 2) and their constituent components (purple in Figure 2) reveals that the GLOSS estimates are indeed averages, and their composition does not precisely correspond to any individual sediment analysis. We also find that the range covered by the GLOSS components is rather limited, from about 50 to 200 ppm ΣREE, whereas our compilation contains analyses ranging an order of magnitude lower and higher at 5 and 5,000 ppm ΣREE, respectively. Additionally, the limited number of GLOSS components overlooks the range in Ce anomalies both at the higher and lower ends of the spectrum. Most GLOSS components and the GLOSS estimates themselves have a negligible to weak negative Ce anomaly.

Carbonatites are notable for their high LREE/HREE ratios, with the cause for such exceptional LREE enrichment currently unknown. It is useful to consider the LREE/HREE ratios in the suggested source material, which we show in Figure 2d using λ_1, the shape coefficient that represents the overall linear slope of a REE pattern. We find that the REE-richest sediments have $\lambda_1 \approx 9$ (equivalent to $[La/Lu]_{CN} \approx 5$), with a strong negative Ce anomaly at roughly Ce/Ce* = 0.2 (as is also evident in Figure 2a). These typically belong to the phosphate-rich sediment type (Ren et al., 2021). On the other hand, the sediments characterized by the strongest LREE/HREE fractionation reach a λ_1 of about 14 (equivalent to $[La/Lu]_{CN} \approx 13$), but they aren't necessarily the richest in REE. They typically have positive Ce anomalies similar to Mn-rich sediments, although not exclusively (i.e., some occasional blue dots appear in the brown dot cloud at the top part of Figure 2d).

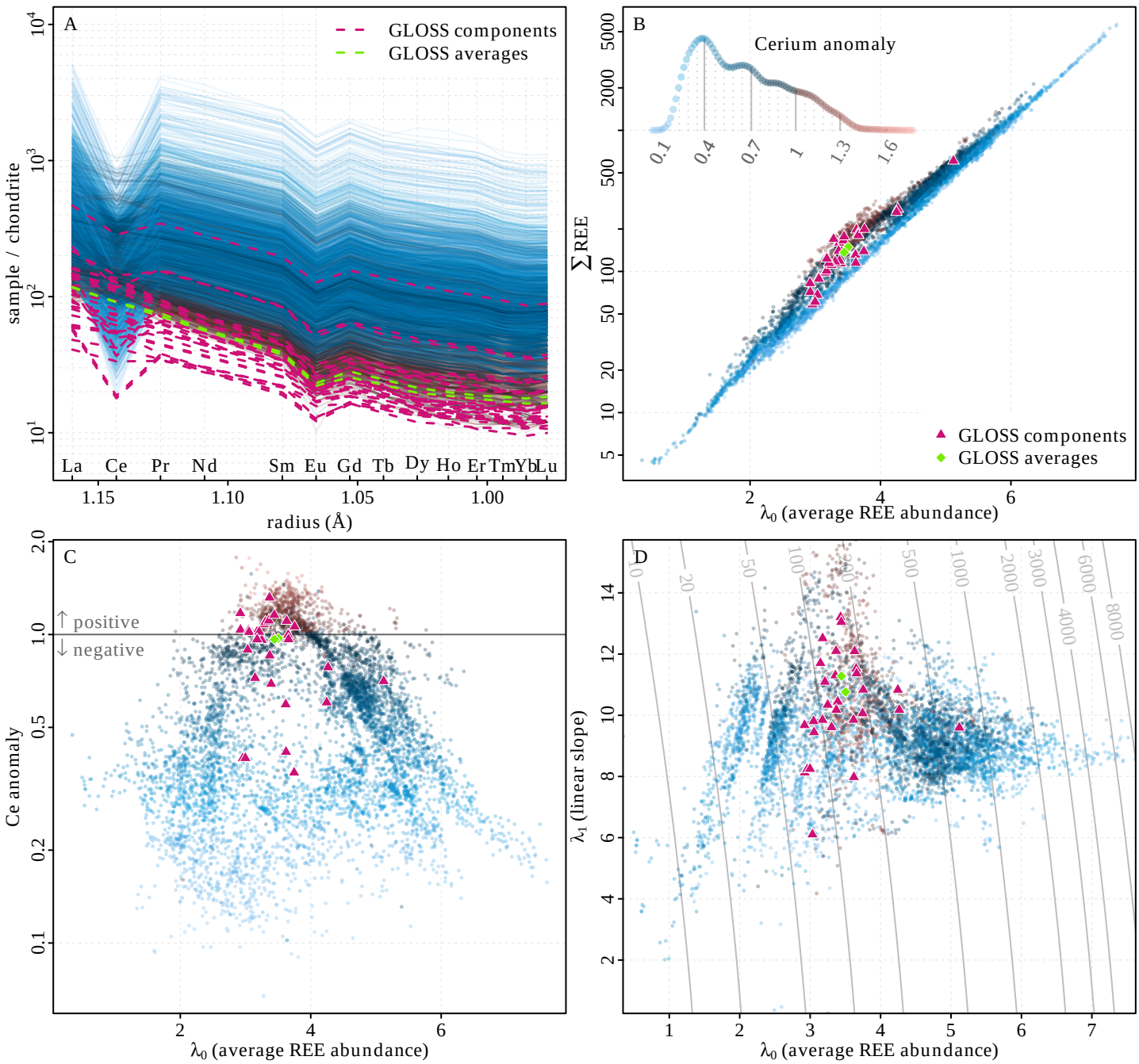

Figure 2. Geochemical characteristics of marine sediments. (a) Chondrite-normalized REE patterns for our global compilation (brown to blue solid lines), GLOSS and GLOSS-II (dashed green lines), and the individual analyses used to derive the GLOSS estimates (dashed purple lines). For this panel only, the data have been filtered to exclude analyses with less than 150 ppm REE because their patterns are typically noisy. (b) Correlation between the λ_0 polynomial shape component (average REE abundance) and total REE abundance of each analysis (ΣREE, in ppm). (c) As above, but the *y*-axis shows calculated Ce anomaly. Unity indicates no anomaly. (d) Lambda-space plot of the global marine sediment data set. Contour lines mark total REE in ppm calculated according to corresponding λ_0 and λ_1, with λ_2 set to 25, and Ce anomalies ignored. For (b)–(d), our compilation in brown to blue solid circles, GLOSS and GLOSS-II in green diamonds, and individual GLOSS components in purple triangles. Cerium anomalies (Ce/Ce*) are color-coded with blue being negative and brown positive according to the inset in (b) that shows a legend with Ce anomalies colors and their frequency distribution curve, applicable to all panels of this figure. Cerium anomalies are derived from the ratio of measured Ce to that expected from the polynomial fit, given as $Ce/Ce^*_{\lambda\tau}$ in Anenburg and Williams (2022). Additional details on the relationship between REE contents and sediment lithology available in Figure 3 of Ren et al. (2021).

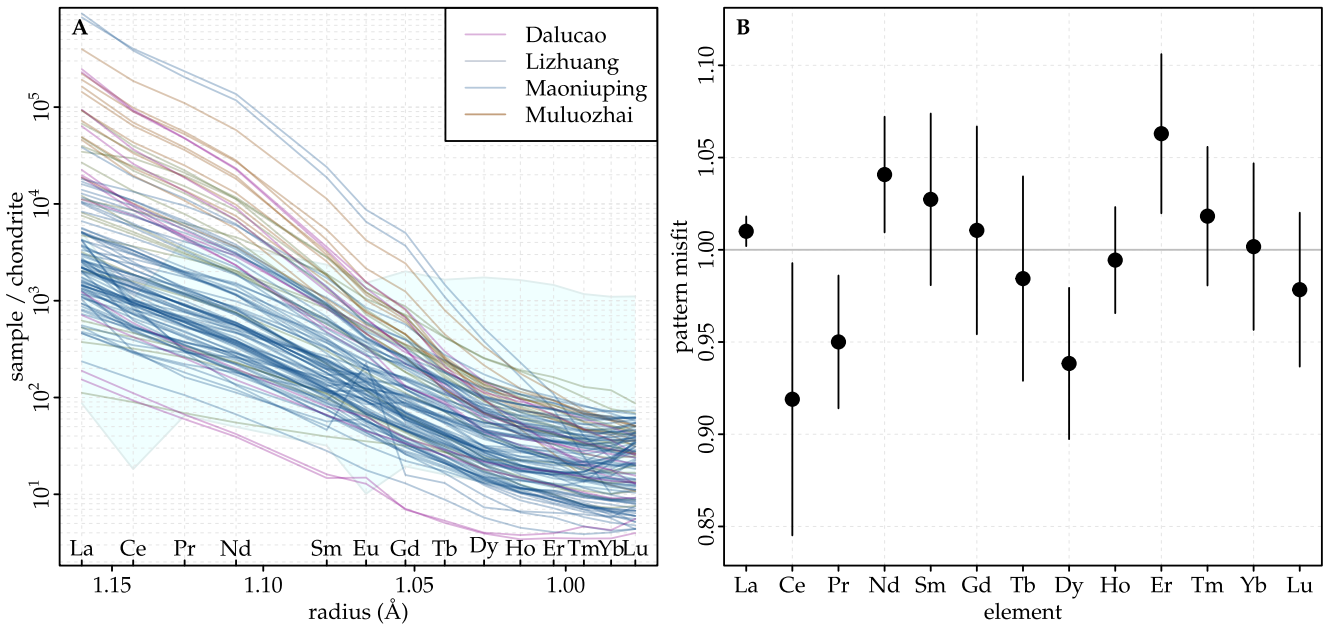

Figure 3. (a) Chondrite-normalized REE patterns for the analyzed Mianning-Dechang rocks in this study, color-coded by individual localities. Shaded area indicates the marine sediment range from Figure 2a. (b) Apparent anomalies derived by dividing measured REE contents and expected REE contents from the lambda polynomial fit. Circles show the mean of all analyses, and error bars show 1σ. Europium is excluded due to possible oxide interferences from the Ba-rich Mianning-Dechang rocks and its redox-sensitive behavior making Eu of little use as a reference point for redox effects on Ce.

3.2. The Mianning-Dechang Carbonatites

Samples from the Mianning-Dechang belt span a variety of rock types, including syenites, carbonatites, anti-skarns, and ore veins (Figure 3a). This was done with the intention of removing bias that might arise from local factors that occurred at a specific sample. Cerium anomalies often derive from near-surface processes under oxidizing conditions, and vary substantially on very short distances. By considering a diverse data set we are able to evaluate whether Ce anomalies (if present) are spatially consistent, thus indicate a Ce-anomalous mantle source. All samples are strongly LREE enriched, with λ_1 values higher than 15 for 99% of analyses ($[La/Lu]_{CN} \approx 16$), and higher than 20 for 95% of analyses ($[La/Lu]_{CN} \approx 39$).

We calculated the average of element misfits relative to a smooth curve (i.e., apparent anomaly) for all samples ($n = 126$). A negative Ce anomaly is observed in the averaged data (~0.92), when measured Ce is ratioed to Ce expected from the polynomial lambda fit ($Ce/Ce^*_{\lambda\tau}$, Figure 3b). Small apparent anomalies are observed for other elements as well (Figure 3b). There is no reason to believe that elements other than Ce (and Eu, excluded from this analysis) should exhibit redox-sensitive anomalies. The misfit of Pr, Dy, and Er is slightly greater than 5%, indicating the possible range of noise.

The most negative misfit is observed for Ce (Figure 3b), potentially indicating a statistically significant Ce anomaly. However, an argument against the presence of a Ce anomaly in the Mianning-Dechang rocks is evident in the weak negative correlation observed between Ce anomalies and pattern slopes (λ_1, Figure 4a). Steeper slopes result from local magmatic differentiation processes, and the steepest slopes likely represent rocks crystallized from low temperature brine-melts (Anenburg et al., 2020, 2021; Yaxley et al., 2022), where a small Ce anomaly might be expected, particularly in oxidized rocks such as the Mianning-Dechang samples (see e.g., Huston et al., 2016; Schlüter et al., 2009). Excluding these highly fractionated samples (of, for instance, $\lambda_1 > 40$) from the average would result in an even weaker Ce anomaly ($Ce/Ce^* \approx 0.94$), which is within the misfit range observed for other elements.

We further investigate whether a Ce anomaly exists for the Mianning-Dechang rocks. This apparent Ce anomaly is linearly correlated with most other anomalies (Table 1), indicating that it results from a misfit between the measured pattern values and the predicted smooth lambda-derived pattern. This is illustrated in Figure 4b, showing data (circles) and polynomial fit (line) for two samples from Mianning-Dechang. The bottom pattern

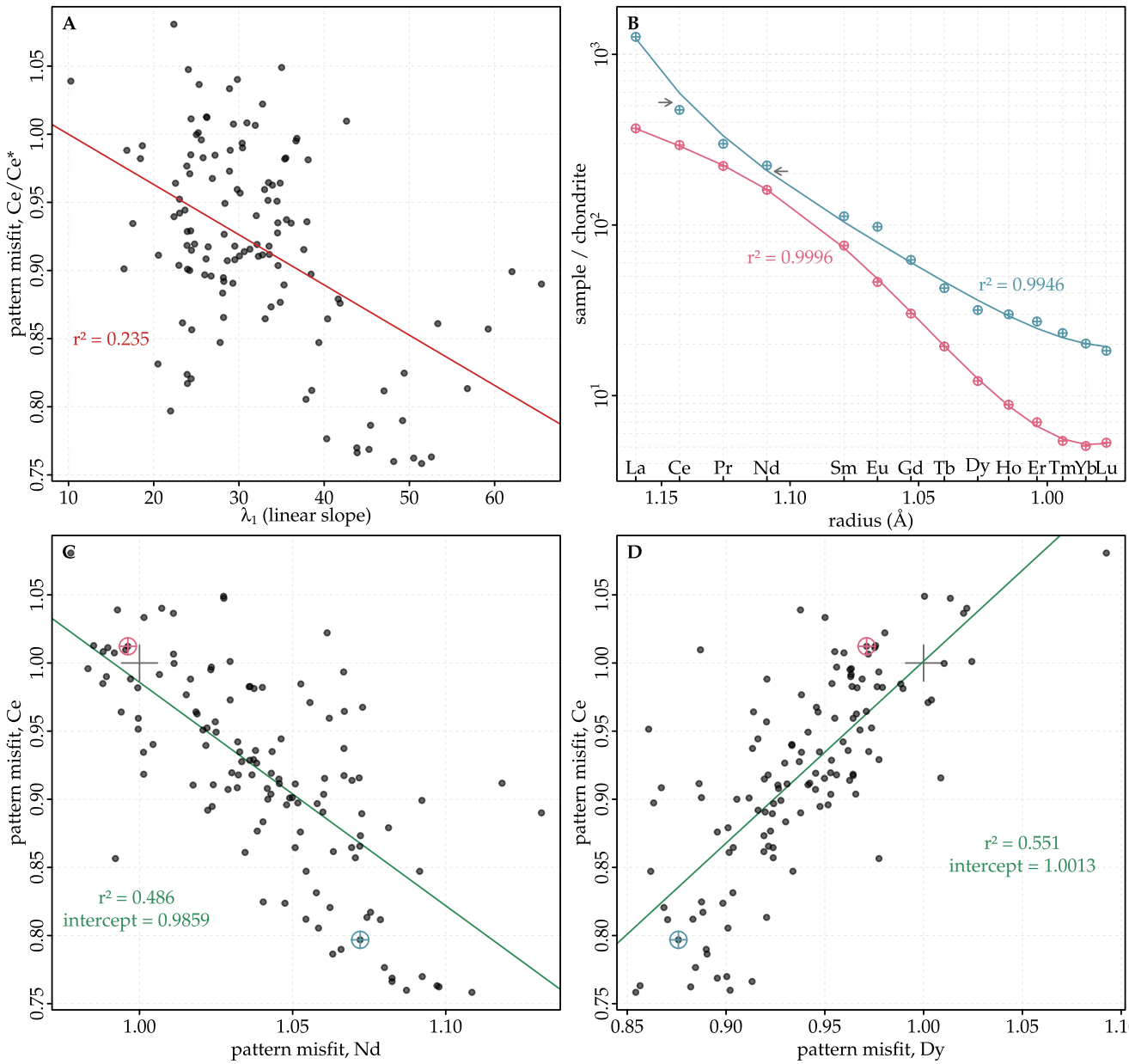

Figure 4. (a) Correlation between the apparent Ce anomaly (pattern misfit) and LREE enrichment in the Mianning-Dechang rocks. The negative Ce anomaly observed in the highest λ_1 patterns can also be visually observed in Figure 3a. (b) Data (symbols) and polynomial fit (lines) for two representative rock analyses from the Mianning-Dechang belt. Arrows indicate mismatch between data and fit in opposite directions. Red pattern has been lowered by 30% to remove overlap between the two patterns and improve clarity. (c, d) Correlation between Ce and Nd or Dy misfits, respectively, for all Mianning-Dechang data. Red and blue analyses from (b) plotted for reference.

(red) has an essentially perfect fit with the observed data. On the other hand, the top pattern (blue) fits well, but not as precise as the former. This causes the curvature to rotate around some elements. For example, the top pattern rotates around the Pr point, with measured Ce slightly lower than the polynomial fit, and Nd slightly higher (as shown by the horizontal arrows). This does not imply a redox-derived anomaly, but simply the fact that a polynomial fit does not capture all complexities of natural data. It also means that over the whole data set, these misfits will be correlated because if the Ce misfit goes up, the Nd misfit must go down. The models predict that the Ce misfits for its surrounding elements La and Pr are 0.9985 and 1.0089 respectively, essentially at unity (Table 1). Elements which are farther away also show this. Figures 4c and 4d show this correlation for a LREE (Nd) and a HREE (Dy), where the predicted misfits occur at 0.9859 and 1.0013 respectively, again very close to

Table 1
Linear Fit Parameters for Apparent Anomalies Between Ce and the Other REE, Sorted by Decreasing r^2

Element	Intercept at Ce/Ce* = 1	r^2
Pr	1.0089	0.771
La	0.9985	0.75
Dy	1.0013	0.551
Tb	0.9336	0.496
Nd	0.9859	0.486
Er	0.9872	0.401
Lu	0.9395	0.288
Tm	0.9373	0.261
Sm	0.9396	0.227
Gd	0.9248	0.175
Yb	0.9197	0.066
Ho	0.9181	0.004

Note. Causes for low r^2 include analytical data spread and presence of outliers. See Supporting Information in https://doi.org/10.6084/m9.figshare.22097921 data files for details on individual elements, and Figures 4c and 4d for an example of correlations around $r^2 \approx 0.5$.

unity. This means that when calculated patterns perfectly fit the measured data, there is no Ce anomaly. When patterns do not fit perfectly, they follow the same trend that indicates the lack of a Ce anomaly, as observed in Figures 4c and 4d. We find that for most elements with a reasonable fit ($r^2 > 0.4$), the predicted Ce anomaly is within the range of 1 ± 0.002 (Table 1), strengthening our view that no significant Ce anomaly is observed in the Mianning-Dechang rocks.

3.3. Other Carbonatites

In addition to the Mianning-Dechang rocks, we examine REE data from three other carbonatites with underlying Phanerozoic mantle metasomatism (Figure 5): Khanneshin in Afghanistan (Tucker et al., 2012), Haast River in New Zealand (Cooper, 2020 and references therein), and Amba Dongar in India (Banerjee & Chakrabarti, 2019). Conducting a thorough REE pattern analysis on these carbonatites—as was done for the Mianning-Dechang rocks above—is not possible because data are overwhelmingly provided as-is with no possibility to explore raw data and apply corrections if necessary. Additionally, data may be acquired using different techniques, in different labs, using a variety of calibration methods. Nonetheless, fitting of these data to lambda coefficients proves useful. Here we choose to fit the data twice, with and without λ_4. Since this coefficient captures a high curvature wavelength, it could potentially lead to bias in noisy data (Figure 5a, Anenburg & Williams, 2022). Assessing both options increases our confidence in the interpretation. Cerium anomalies for REE patterns from all three carbonatites are given in Figure 5b and show a strong variability. On average, fits with λ_4 show a weak positive Ce anomaly (Ce/Ce* ≈ 1.08–1.09) and fits without λ_4 show a weak negative to no Ce Anomaly (Ce/Ce* ≈ 0.95–1.00). A one standard deviation interval from the mean includes Ce/Ce* = 1 in five out of these six cases (two calculation methods for three carbonatites). The only exception is Amba Dongar using λ_4, where the lowest value is a positive anomaly at 1.05 (Figure 5b), the opposite of a presumed negative anomaly expected for REE-rich sediments. This exercise has been also attempted for the Bear Lodge carbonatite in Wyoming, USA (Moore et al., 2015). The mantle source for the Bear Lodge carbonatite

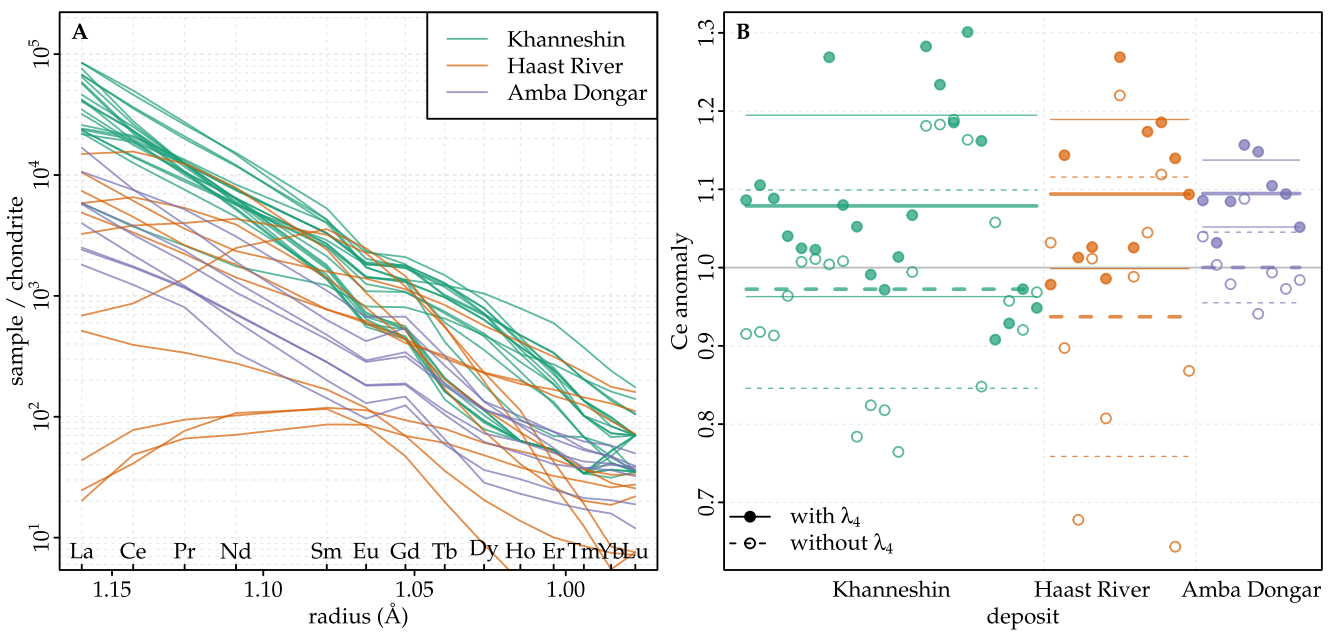

Figure 5. (a) Chondrite-normalized REE patterns for three Phanerozoic carbonatites. (b) Ce anomalies as calculated by the misfit of measured Ce and the fitted pattern based on lambda coefficients, with and without including λ_4 in the fitting process. Data from Tucker et al. (2012), Cooper (2020), and Banerjee and Chakrabarti (2019). Thick lines indicate mean values, and two thin lines indicate means ± one standard deviations.

experienced EM1-type Cretaceous to Eocene subduction metasomatism. Unfortunately, the REE data given by Moore et al. (2015) are rather noisy and poorly fit the polynomial shapes, such that fits including or excluding λ_4 result in average Ce anomalies of 1.25 and 0.83, respectively. In any case, a visual inspection of the patterns and calculation of Ce anomalies via the interpolation method reveals no obviously conspicuous Ce anomalies (Moore et al., 2015, see their corrigendum for Ce anomaly values).

4. Discussion

Our marine sediment compilation can be roughly divided into three components (Figure 2d). The first is Ce-neutral to negatively anomalous and REE-poor (up to ~100 ppm, left of Figure 2d and omitted from Figure 2a for clarity). This component is likely dominated by carbonate (e.g., Y. Deng, Guo, et al., 2022), and complementary to the second component with positive Ce-anomalies and 100–200 ppm REE (Figure 2d), represented by Mn-oxide and Fe-oxide nodules (Cao et al., 2020). Taken together, these two components contain approximately the same REE contents as GLOSS (~150 ppm) (Plank, 2014). The third component is REE-rich (>200 to ~8,000 ppm), and has a conspicuous negative Ce anomaly. These sediments are often dominated by a phosphate component (Ren et al., 2021, 2022; Yasukawa et al., 2014; X. Zhang et al., 2017). It is this third phosphate component that is occasionally implicated in the exceptional REE contents of the Mianning-Dechang belt deposits (Weng et al., 2021; Zhu et al., 2024). Evidence for REE recycling through subduction exists elsewhere—Ce anomalies have been observed to be recycled from subducted marine sediments to the overlying volcanic arc in the Mariana trench. The Mariana sediments span a range of Ce anomalies, as low as Ce/Ce* ≈ 0.5, and volcanic rocks inherit some of that signal with Ce/Ce* values in lavas reaching 0.9 (Bellot et al., 2018). We note that the detection of Ce-anomalous magmatic rocks through subducted sediments is a challenging endeavor, and often leads to inconclusive results (Bellot et al., 2015; Israel et al., 2020). Evidently, some sedimentary Ce anomalies can be recycled through subduction into derived igneous rocks. Any magmatic processes that might take a Ce-negative source and serendipitously cancel that anomaly are implausible, with the implication that if Ce anomalies exist in the same REE component that is being recycled, then the anomalies are likewise expected in the newly formed carbonatites.

4.1. Cerium Anomalies During the Neoproterozoic

The discussion up to this point focused on modern marine sediments. However, the subduction zone thought to fertilize the mantle underneath Mianning-Dechang operated during the Neoproterozoic, at roughly 800–700 Ma (Guo et al., 2005). As Ce anomalies in marine sediments did not remain constant throughout Earth's history, it is useful to test whether REE-rich marine sediments—including phosphatic sediments—subducted during the Neoproterozoic had a similar negative Ce anomaly. The separation of Ce from the other REE requires oxidized conditions which developed in the mid-Proterozoic (Bellefroid et al., 2018; Tang et al., 2016; K. Zhang & Shields, 2022). A global review of marine carbonate sediments shows that by the beginning of the Neoproterozoic at 1.0 Ga, their Ce/Ce* values were as low as 0.8–0.7, with more negative values of 0.6 developing throughout the era (X. M. Liu et al., 2021). Although these data represent carbonates rather than REE-rich phosphates, our data for modern sediments indicates that Ce anomalies for both carbonates and phosphates are typically within the same range. Negative Ce anomalies are well known from many Neoproterozoic Chinese localities (S. Chen et al., 2014). Data on Neoproterozoic phosphate is less common, but examples of substantial negative Ce anomalies, down to 0.6, exist from China (Xin et al., 2015, 2016) and elsewhere (Frei et al., 2017; Gómez-Peral et al., 2014, 2017; Krupenin et al., 2023; Mazumdar et al., 2003; Shields & Stille, 1998). Although these Ce anomalies are much weaker than modern anomalies which reach negative anomalies of up to 0.1, they still denote that up to 40% of the Ce is missing from these deposits. Locally, the Proterozoic Kunyang Group is a sedimentary sequence commonly believed to represent material subducted underneath the future Mianning-Dechang carbonatite belt (H. Liu et al., 2020). Sedimentary carbonate rocks from the Fengshan member of the Kunyang Group show Ce/Ce* = 0.76 (Y. Yang, 2003). Samples from the clastic sediment formations of the Kunyang Group typically show a positive correlation between phosphate contents, total REE, and the magnitude of the negative Ce anomaly, reaching values as low as Ce/Ce* = 0.77 (Ji et al., 2016). Ubiquitous Ce anomalies in REE-rich marine sediments and the complete lack of such anomalies in the Mianning-Dechang rocks strongly suggests that REE from marine sediments did not find their way into the carbonatites and related rocks. Had these marine sediments been recycled as the primary contributors to the REE budget of the carbonatites, a statistically significant Ce anomaly should have been inherited, but no such anomaly is observed (Figure 3).

4.2. Carbonatites With Underlying Phanerozoic Metasomatism

The combined presence of Ce anomalies in some subduction zone sediments and lack of Ce anomalies in overlying carbonatites is not unique to the Mianning-Dechang belt. To further demonstrate the point, we choose three Phanerozoic carbonatites (Figure 5). Importantly, mantle metasomatism preceding carbonatite rock formation has also been shown to be Phanerozoic, removing uncertainties on whether Ce anomalies existed in the subducted sediments. An instructive example is that of the Khanneshin carbonatite volcano in Afghanistan, shown to derive from marine sediments deposited at 29 Ma (Horton, 2021). These marine sediments were subducted through the Makran subduction zone. Their composition is probably similar to modern marine sediments deposited on the north Indian Ocean and Arabian Sea. Some of these sediments have been shown previously to contain negative Ce anomalies, typically $Ce/Ce^* \approx 0.8$ (Nagender et al., 1997; Pattan & Higgs, 1995; Rao et al., 2008; Sirocko, 2000; Yasukawa et al., 2014), which are not as extreme as some sediments in our compilation (e.g., down to 0.1). Nonetheless, a shortage of roughly 20% Ce from the potential source material for REE mineralization is expected to be appear in the deposit as well. Although these anomalous sediments are not representative of the Makran sediments as a whole (Plank, 2014), the hypothesis that phosphatic REE-rich sediments in particular are recycled to carbonatites requires a similar anomaly at Khanneshin. However, REE patterns of the Khanneshin rocks are smooth, lacking any Ce anomalies (Figure 5, Tucker et al., 2012).

Haast River, New Zealand, is a carbonatite that intruded as part of a wider Cenozoic province of alkaline rocks (Cooper, 2020). Amba Dongar, Gujarat, India, is a carbonatite that is related to the Deccan Traps (Chandra et al., 2017), intruded around the Mesozoic–Cenozoic boundary, and is particularly known for its potentially economic mineralization of REE, fluorite, and Nb (Dhote et al., 2021; Patel et al., 2022; Viladkar & Sorokhtina, 2021). For both carbonatites, mantle metasomatism occurred in the Mesozoic (Banerjee & Chakrabarti, 2019; Chandra et al., 2017; McCoy-West et al., 2016; van der Meer et al., 2017), at a time when Ce-anomalous sediments were widespread on the sea floor (K. Zhang & Shields, 2022). A similar scenario occurred for the Bear Lodge carbonatite (Moore et al., 2015). As above, a Ce anomaly is to be expected had the REE-rich sediments contributed to the REE budget of the carbonatites, but no Ce anomaly is observed (Figure 5b). This indicates that the Ce-anomalous and REE-rich sediments are not the source of the REE in all three Phanerozoic carbonatites considered here, in line with our findings for the Mianning-Dechang carbonatites.

4.3. What Is the REE Source?

The concept that mantle fertilization is a prerequisite for ore deposit formation is widespread and has been applied to many ore deposit types (Blanks et al., 2020; Hou et al., 2023; Spandler et al., 2020; Tassara et al., 2017). There is no doubt that elevated REE contents within carbonatite mantle sources are beneficial; the average primitive mantle contains less than 1 ppm La (Palme & O'Neill, 2014), whereas average subducting sediments contain almost 30 ppm (Plank, 2014). There is compelling evidence that metasomatism driven by carbonated sediment melting occurs (C. Chen et al., 2016, 2017; Hoernle et al., 2002), but the question of whether this is required for economic REE mineralization remains open. Claims of "metasomatism" or "refertilization" do not always contribute to the answer, as different elements will have different mobilities in mantle conditions, such that metasomatism may contribute elements other than the REE (e.g., Amsellem et al., 2023; Bolhar et al., 2020). The fact that metasomatism introduced carbonate and perhaps Ca, Mg, Sr, or alkalis, does not necessarily mean that REE were likewise enriched. For example, Boyet et al. (2019) studied rocks with a negative Ce anomaly (down to 0.92) and an enriched mantle (EM1) isotopic signature, but could not find a clear subducted-sediment contribution to the observed Ce anomaly. At most, Boyet et al. (2019) suggest 2% sediment contribution of La and Ce (and by extension, the entire REE series) to the mantle source. If correct, this amount is negligible and the sediment REE contents would be diluted to those of the ambient mantle. Our finding that REE-rich sediments are not necessary raises a question of whether sediment subduction is important at all. Although small REE-enrichments are likely beneficial and propagate to crustal magmatic differentiation and mineralization, not all deposits show this kind of enriched signature. Demonstrably, giant carbonatite-hosted REE deposits can form without any mantle enrichment or metasomatism by subducting sediments (Mount Weld in Western Australia being the most notable example of this, Chandler et al., 2024; Nelson et al., 1988), in addition to the finding that carbonatites, in general, do not require recycled sediments (Sun et al., 2021).

Most carbonatite melts are understood to form by low degree partial melting of carbonated mantle rocks (Hammouda & Keshav, 2015; Pintér et al., 2021), often with additional alkalis added by metasomatism (Thomsen

& Schmidt, 2008). Carbonatites rarely form during or immediately after subduction (Grassi & Schmidt, 2010; Thomsen & Schmidt, 2008; Tsuno et al., 2012). They form by either direct mantle melting, or immiscible separation from a carbonated silicate melt (Yaxley et al., 2021), with melt formation often occurring several hundreds of millions of year after subduction has ceased (Yaxley et al., 2022). The Mianning-Dechang carbonatites are an excellent example of this time gap (Hou et al., 2023). Even when melting occurs (e.g., X. Y. Zhang et al., 2022), REE may remain refractory and immobile (Zhu et al., 2024). In this case, a single "lump" of phosphatic REE-rich material is unlikely to be wholly mobilized into a carbonated mantle melt. We note that the REE mineral hosts in sediments (i.e., phosphates, carbonates, or Mn-nodules) are unlikely to exert significant control on REE partitioning during melting processes. The REE will partition between high temperature phases, equilibrated over a large volume of material facilitated by the presence of melts and fluids. Moreover, a thin REE-rich sedimentary veneer of several tens of meters on top of a full km-scale section of crust will contribute a negligible REE amount to the total subducted REE budget. Protracted subduction will stir and mix these REE-rich domains, and probably smear them over large spatial extents, such that the REE-rich material is diluted by other, more average rocks, that subducted before or after it. Any REE that partitions to carbonatite-forming melts are therefore likely to be sourced from an averaged, large volume, mantle source, while noting that only low melt fractions actually form across this extent (Pintér et al., 2021). This average continental crust will have a negligible negative Ce anomaly ($Ce/Ce^* = 0.97$, W. Li, Nakada, et al., 2023), and its contribution is unlikely to be amenable to detection by the Ce-anomaly method in carbonatites. Nonetheless, using misfit correlations trends, we were able to determine (Figures 4c and 4d) that the Ce anomaly in the Mianning-Dechang rocks is essentially 1.00. If the W. Li, Nakada, et al. (2023) data set is as precise, then our study not only rejects the significant presence of unusually REE-rich phosphatic sediments in carbonatite mantle sources, but also raises a question on whether any REE in continental-derived marine sediments contributes a substantial amount to REE ore deposits.

Our view is that most carbonatite melts have the potential to evolve to high REE contents regardless of their mantle source. This results from several processes that preferentially concentrate REE into carbonatite melts. First, REE will strongly partition to primary mantle-derived carbonatite melts (Foley et al., 2009). Second, carbonatite melts strongly sequester REE when form by immiscibility (Nabyl et al., 2020, 2021). Third, when a carbonatite melt reaches the upper crust and begins differentiating, REE are highly incompatible and will be strongly enriched in residual brine-melts (Anenburg et al., 2020, 2021). Each of these processes will cause one or more orders of magnitude increase in carbonatite melt REE contents. Combined, these processes can lead to high grade mineralization. Mineralized portions of carbonatites are often volumetrically small relative to the entire carbonatite system that hosts them (Anenburg et al., 2021). Rare earth element enrichment and concentration by magmatic differentiation is now well established for most economic REE deposits (Chandler et al., 2024; Chikanda et al., 2019; Feng et al., 2020; X.-C. Li et al., 2024; Song et al., 2023; K. Yang et al., 2019; Zheng et al., 2023), suggesting that the role of subducted REE-rich sediments at source may only be secondary. In our preferred scenario, a mantle source with negligible Ce anomalies undergoes partial melting. This melt evolves at high temperature conditions which overwhelmingly stabilize Ce^{3+}. Late-stage differentiation results in REE mineralization without any notable Ce anomalies, as is predominantly observed in nature. Given that carbonatite systems are known for their vertical variability (Frolov, 1971; Vasyukova & Williams-Jones, 2022; Walter et al., 2021), whether any single carbonatite is economic or not may have little to do with mantle fertilization, but rather the happenstance of its REE-rich domains found at or near the modern erosion surface.

5. Conclusions

The previously suggested model for formation of giant REE-deposits within the Mianning-Dechang carbonatites invokes recycling of subducted REE-rich marine sediments (Hou et al., 2015, 2023; Weng et al., 2021). Here, we show that REE-rich marine sediments, compared to average marine sediments, are characterized by a strong negative Ce anomaly. This has been the case since the Neoproterozoic, the time in which the mantle underlying the Mianning-Dechang belt has been fertilized by subduction. If these REE-rich sediments were supposedly recycled into the carbonatite-associated deposits, then a similar Ce anomaly should exist in the rocks as well. However, no such anomaly is observed in our Mianning-Dechang chemical analyses. Therefore, exceptionally REE-rich marine sediments are unlikely to be the source of the REE themselves, despite the ubiquitous sedimentary isotopic signature (Yaxley et al., 2022). A question remains regarding the ultimate source of the REE in the Mianning-Dechang belt and other deposits for which a similar model was proposed.

The answer is beyond the scope of this work, and will most likely require a combination of experimental, analytical, and theoretical studies.

Conflict of Interest

The authors declare no conflicts of interest relevant to this study.

Data Availability Statement

Supplementary data including the full marine sediment compilation, raw Mianning-Dechang data, and reused Phanerozoic carbonatite data are available in an R notebook (R Core Team, 2023). With all data processing required to generate all figures is available at *figshare* (Anenburg & Liu, 2024). The script generates a cleaned, merged and corrected data set for the Mianning-Dechang rocks (`dat_merged.csv`), which is also available in the *figshare* repository and intended for reuse in future studies.

Acknowledgments
This study was supported by the Second Tibetan Plateau Scientific Expedition and Research (Grant 2021QZKK0304), National Natural Science Foundation of China (92162216), and the Australian Research Council (Linkage Grant LP190100635). We appreciate constructive and useful reviews by Charles D. Beard, Nicholas D. Barber and Associate Editor Susanne Straub. Open access publishing facilitated by Australian National University, as part of the Wiley - Australian National University agreement via the Council of Australian University Librarians.

References

Amsellem, E., Schiller, M., Klausen, M., Bouyon, A., Rojas, V., & Bizzarro, M. (2023). Origin of carbonatites and associated silicate rocks revealed by Mg triple-isotope approach. *Chemical Geology*, *636*, 121663. https://doi.org/10.1016/j.chemgeo.2023.121663

Andersen, T. (1987). Mantle and crustal components in a carbonatite complex, and the evolution of carbonatite magma: REE and isotopic evidence from the Fen complex, southeast Norway. *Chemical Geology: Isotope Geoscience section*, *65*(2), 147–166. https://doi.org/10.1016/0168-9622(87)90070-4

Anenburg, M. (2020). Rare earth mineral diversity controlled by REE pattern shapes. *Mineralogical Magazine*, *84*(5), 629–639. https://doi.org/10.1180/mgm.2020.70

Anenburg, M., Broom-Fendley, S., & Chen, W. (2021). Formation of rare earth deposits in carbonatites. *Elements*, *17*(5), 327–332. https://doi.org/10.2138/gselements.17.5.327

Anenburg, M., & Liu, Y. (2024). Bulk rock geochemical analyses for carbonatites and related rocks from Mianning-Dechang, China [Dataset]. *figshare*. https://doi.org/10.6084/m9.figshare.22097921

Anenburg, M., Mavrogenes, J. A., Frigo, C., & Wall, F. (2020). Rare earth element mobility in and around carbonatites controlled by sodium, potassium, and silica. *Science Advances*, *6*(41), eabb6570. https://doi.org/10.1126/sciadv.abb6570

Anenburg, M., & Williams, M. J. (2022). Quantifying the tetrad effect, shape components, and Ce–Eu–Gd anomalies in rare earth element patterns. *Mathematical Geosciences*, *54*(1), 47–70. https://doi.org/10.1007/s11004-021-09959-5

Banerjee, A., & Chakrabarti, R. (2019). A geochemical and Nd, Sr and stable Ca isotopic study of carbonatites and associated silicate rocks from the ~65 Ma old Ambadongar carbonatite complex and the Phenai Mata igneous complex, Gujarat, India: Implications for crustal contamination, carbonate recycling, hydrothermal alteration and source-mantle mineralogy. *Lithos*, *326–327*, 572–585. https://doi.org/10.1016/j.lithos.2019.01.007

Barrat, J.-A., Bayon, G., & Lalonde, S. (2023). Calculation of cerium and lanthanum anomalies in geological and environmental samples. *Chemical Geology*, *615*, 121202. https://doi.org/10.1016/j.chemgeo.2022.121202

Bell, K., & Tilton, G. R. (2001). Nd, Pb and Sr isotopic compositions of east African carbonatites: Evidence for mantle mixing and plume inhomogeneity. *Journal of Petrology*, *42*(10), 1927–1945. https://doi.org/10.1093/petrology/42.10.1927

Bellefroid, E. J., Hood, A. V. S., Hoffman, P. F., Thomas, M. D., Reinhard, C. T., & Planavsky, N. J. (2018). Constraints on Paleoproterozoic atmospheric oxygen levels. *Proceedings of the National Academy of Sciences*, *115*(32), 8104–8109. https://doi.org/10.1073/pnas.1806216115

Bellot, N., Boyet, M., Doucelance, R., Bonnand, P., Savov, I. P., Plank, T., & Elliott, T. (2018). Origin of negative cerium anomalies in subduction-related volcanic samples: Constraints from Ce and Nd isotopes. *Chemical Geology*, *500*, 46–63. https://doi.org/10.1016/j.chemgeo.2018.09.006

Bellot, N., Boyet, M., Doucelance, R., Pin, C., Chauvel, C., & Auclair, D. (2015). Ce isotope systematics of island arc lavas from the Lesser Antilles. *Geochimica et Cosmochimica Acta*, *168*, 261–279. https://doi.org/10.1016/j.gca.2015.07.002

Blanks, D. E., Holwell, D. A., Fiorentini, M. L., Moroni, M., Giuliani, A., Tassara, S., et al. (2020). Fluxing of mantle carbon as a physical agent for metallogenic fertilization of the crust. *Nature Communications*, *11*(1), 4342. https://doi.org/10.1038/s41467-020-18157-6

Bolhar, R., Whitehouse, M. J., Milani, L., Magalhães, N., Golding, S. D., Bybee, G., et al. (2020). Atmospheric S and lithospheric Pb in sulphides from the 2.06 Ga Phalaborwa phoscorite-carbonatite Complex, South Africa. *Earth and Planetary Science Letters*, *530*, 115939. https://doi.org/10.1016/j.epsl.2019.115939

Boyet, M., Doucelance, R., Israel, C., Bonnand, P., Auclair, D., Suchorski, K., & Bosq, C. (2019). New constraints on the origin of the EM-1 component revealed by the measurement of the La-Ce isotope systematics in Gough Island lavas. *Geochemistry, Geophysics, Geosystems*, *20*(5), 2484–2498. https://doi.org/10.1029/2019gc008228

Burnham, A. D., & Berry, A. J. (2014). The effect of oxygen fugacity, melt composition, temperature and pressure on the oxidation state of cerium in silicate melts. *Chemical Geology*, *366*, 52–60. https://doi.org/10.1016/j.chemgeo.2013.12.015

Cao, C., Liu, X.-M., Bataille, C. P., & Liu, C. (2020). What do Ce anomalies in marine carbonates really mean? A perspective from leaching experiments. *Chemical Geology*, *532*, 119413. https://doi.org/10.1016/j.chemgeo.2019.119413

Chandler, R., Bhat, G., Mavrogenes, J., Knell, B., David, R., & Leggo, T. (2024). The primary geology of the Paleoproterozoic Mt Weld carbonatite complex, Western Australia. *Journal of Petrology*, *65*(2), egae007. https://doi.org/10.1093/petrology/egae007

Chandra, J., Paul, D., Viladkar, S. G., & Sensarma, S. (2017). Origin of the Amba Dongar carbonatite complex, India and its possible linkage with the Deccan Large Igneous Province. *Geological Society, London, Special Publications*, *463*(1), 137–169. https://doi.org/10.1144/sp463.3

Chen, C., Liu, Y., Foley, S. F., Ducea, M. N., Geng, X., Zhang, W., et al. (2017). Carbonated sediment recycling and its contribution to lithospheric refertilization under the northern North China Craton. *Chemical Geology*, *466*, 641–653. https://doi.org/10.1016/j.chemgeo.2017.07.016

Chen, C., Liu, Y., Foley, S. F., Ducea, M. N., He, D., Hu, Z., et al. (2016). Paleo-Asian oceanic slab under the North China craton revealed by carbonatites derived from subducted limestones. *Geology*, *44*(12), 1039–1042. https://doi.org/10.1130/g38365.1

Chen, S., Gui, H., & Sun, L. (2014). Geochemical characteristics of REE in the Late Neo-proterozoic limestone from northern Anhui Province, China. *Chinese Journal of Geochemistry*, *33*(2), 187–193. https://doi.org/10.1007/s11631-014-0677-z

Chikanda, F., Otake, T., Ohtomo, Y., Ito, A., Yokoyama, T. D., & Sato, T. (2019). Magmatic-hydrothermal processes associated with rare earth element enrichment in the Kangankunde carbonatite complex, Malawi. *Minerals*, *9*(7), 442. https://doi.org/10.3390/min9070442

Cooper, A. F. (2020). Petrology and petrogenesis of an intraplate alkaline lamprophyre-phonolite-carbonatite association in the Alpine Dyke Swarm, New Zealand. *New Zealand Journal of Geology and Geophysics*, *63*(4), 469–488. https://doi.org/10.1080/00288306.2019.1684324

Deng, J., Wang, Q., Sun, X., Yang, L., Groves, D. I., Shu, Q., et al. (2022). Tibetan ore deposits: A conjunction of accretionary orogeny and continental collision. *Earth-Science Reviews*, *235*, 104245. https://doi.org/10.1016/j.earscirev.2022.104245

Deng, Y., Guo, Q., Zhu, J., He, G., Yang, Y., Cao, J., et al. (2022). Significant contribution of seamounts to the oceanic rare earth elements budget. *Gondwana Research*, *112*, 71–81. https://doi.org/10.1016/j.gr.2022.09.016

Deng, Y., Ren, J., Guo, Q., Cao, J., Wang, H., & Liu, C. (2018). Geochemistry characteristics of REY-rich sediment from deep sea in Western Pacific, and their indicative significance. *Acta Petrologica Sinica*, *34*(3), 733–747. Retrieved from https://oversea.cnki.net/kcms/detail/detail.aspx?dbcode=CJFD&filename=YSXB201803013

Dhote, P., Bhan, U., & Verma, D. (2021). Genetic model of carbonatite hosted rare earth elements mineralization from Ambadongar Carbonatite Complex, Deccan Volcanic Province, India. *Ore Geology Reviews*, *135*, 104215. https://doi.org/10.1016/j.oregeorev.2021.104215

Ding, C., Zhao, B., Dai, P., Li, D., Zhang, Z., Sun, R., et al. (2022). Geochronology, geochemistry and Sr–Nd–Pb–Hf isotopes of the alkaline–carbonatite complex in the Weishan REE deposit, Luxi Block: Constraints on the genesis and tectonic setting of the REE mineralization. *Ore Geology Reviews*, *147*, 104996. https://doi.org/10.1016/j.oregeorev.2022.104996

Feng, M., Song, W., Kynicky, J., Smith, M., Cox, C., Kotlanova, M., et al. (2020). Primary rare earth element enrichment in carbonatites: Evidence from melt inclusions in Ulgii Khiid carbonatite, Mongolia. *Ore Geology Reviews*, *117*, 103294. https://doi.org/10.1016/j.oregeorev.2019.103294

Foley, S. F., Yaxley, G. M., Rosenthal, A., Buhre, S., Kiseeva, E. S., Rapp, R. P., & Jacob, D. E. (2009). The composition of near-solidus melts of peridotite in the presence of CO_2 and H_2O between 40 and 60 kbar. *Lithos*, *112*, 274–283. https://doi.org/10.1016/j.lithos.2009.03.020

Frei, R., Døssing, L. N., Gaucher, C., Boggiani, P. C., Frei, K. M., Bech Árting, T., et al. (2017). Extensive oxidative weathering in the aftermath of a late Neoproterozoic glaciation—Evidence from trace element and chromium isotope records in the Urucum district (Jacadigo Group) and Puga iron formations (Mato Grosso do Sul, Brazil). *Gondwana Research*, *49*, 1–20. https://doi.org/10.1016/j.gr.2017.05.003

Frolov, A. A. (1971). Vertical zonation in deposition of ore, as in ultrabasic-alkaline rocks and carbonatites. *International Geology Review*, *13*(5), 685–695. https://doi.org/10.1080/00206817109475486

Gao, L.-G., Chen, Y.-W., Bi, X.-W., Gao, J.-F., Chen, W. T., Dong, S.-H., et al. (2021). Genesis of carbonatite and associated U–Nb–REE mineralization at Huayangchuan, central China: Insights from mineral paragenesis, chemical and Sr-Nd-C-O isotopic compositons of calcite. *Ore Geology Reviews*, *138*, 104310. https://doi.org/10.1016/j.oregeorev.2021.104310

Gómez-Peral, L. E., Kaufman, A. J., & Poiré, D. G. (2014). Paleoenvironmental implications of two phosphogenic events in Neoproterozoic sedimentary successions of the Tandilia System, Argentina. *Precambrian Research*, *252*, 88–106. https://doi.org/10.1016/j.precamres.2014.07.009

Gómez-Peral, L. E., Sial, A. N., Arrouy, M. J., Richiano, S., Ferreira, V. P., Kaufman, A. J., & Poiré, D. G. (2017). Paleo-climatic and paleo-environmental evolution of the Neoproterozoic basal sedimentary cover on the Río de La Plata Craton, Argentina: Insights from the $\delta^{13}C$ chemostratigraphy. *Sedimentary Geology*, *353*, 139–157. https://doi.org/10.1016/j.sedgeo.2017.03.007

Goodenough, K. M., Deady, E. A., Beard, C. D., Broom-Fendley, S., Elliott, H. A. L., van den Berg, F., & Öztürk, H. (2021). Carbonatites and alkaline igneous rocks in post-collisional settings: Storehouses of rare earth elements. *Journal of Earth Science*, *32*(6), 1332–1358. https://doi.org/10.1007/s12583-021-1500-5

Grabarczyk, A., Gil, G., Liu, Y., Kotowski, J., Jokubauskas, P., Barnes, J. D., et al. (2022). Ultramafic-alkaline-carbonatite Tajno intrusion in NE Poland: A new hypothesis about the massif formation and related mineralization. *Ore Geology Reviews*, *143*, 104772. https://doi.org/10.1016/j.oregeorev.2022.104772

Grassi, D., & Schmidt, M. W. (2010). Melting of carbonated pelites at 8–13 GPa: Generating K-rich carbonatites for mantle metasomatism. *Contributions to Mineralogy and Petrology*, *162*(1), 169–191. https://doi.org/10.1007/s00410-010-0589-9

Guarino, V., Wu, F.-Y., Melluso, L., de Barros Gomes, C., Tassinari, C. C. G., Ruberti, E., & Brilli, M. (2017). U–Pb ages, geochemistry, C–O–Nd–Sr–Hf isotopes and petrogenesis of the Catalão II carbonatitic complex (Alto Paranaíba Igneous Province, Brazil): Implications for regional-scale heterogeneities in the Brazilian carbonatite associations. *International Journal of Earth Sciences*, *106*(6), 1963–1989. https://doi.org/10.1007/s00531-016-1402-4

Guo, Z., Hertogen, J., Liu, J., Pasteels, P., Boven, A., Punzalan, L., et al. (2005). Potassic magmatism in Western Sichuan and Yunnan Provinces, SE Tibet, China: Petrological and geochemical constraints on petrogenesis. *Journal of Petrology*, *46*(1), 33–78. https://doi.org/10.1093/petrology/egh061

Hammouda, T., & Keshav, S. (2015). Melting in the mantle in the presence of carbon: Review of experiments and discussion on the origin of carbonatites. *Chemical Geology*, *418*, 171–188. https://doi.org/10.1016/j.chemgeo.2015.05.018

Hoernle, K., Tilton, G., Le Bas, M. J., Duggen, S., & Garbe-Schönberg, D. (2002). Geochemistry of oceanic carbonatites compared with continental carbonatites: Mantle recycling of oceanic crustal carbonate. *Contributions to Mineralogy and Petrology*, *142*(5), 520–542. https://doi.org/10.1007/s004100100308

Horton, F. (2021). Rapid recycling of subducted sedimentary carbon revealed by Afghanistan carbonatite volcano. *Nature Geoscience*, *14*(7), 508–512. https://doi.org/10.1038/s41561-021-00764-7

Hou, Z. Q., Liu, Y., Tian, S., Yang, Z., & Xie, Y. (2015). Formation of carbonatite-related giant rare-earth-element deposits by the recycling of marine sediments. *Scientific Reports*, *5*(1), 10231. https://doi.org/10.1038/srep10231

Hou, Z.-Q., Xu, B., Zhang, H., Zheng, Y.-C., Wang, R., Liu, Y., et al. (2023). Refertilized continental root controls the formation of the Mianning–Dechang carbonatite-associated rare-earth-element ore system. *Communications Earth & Environment*, *4*(1), 293. https://doi.org/10.1038/s43247-023-00956-6

Hussain, A., Zhao, K.-D., Arif, M., Palmer, M. R., Chen, W., Zhang, Q., et al. (2020). Geochronology, mineral chemistry and genesis of REE mineralization in alkaline rocks from the Kohistan Island Arc, Pakistan. *Ore Geology Reviews*, *126*, 103749. https://doi.org/10.1016/j.oregeorev.2020.103749

Huston, D. L., Maas, R., Cross, A., Hussey, K. J., Mernagh, T. P., Fraser, G., & Champion, D. C. (2016). The Nolans Bore rare-earth element-phosphorus-uranium mineral system: Geology, origin and post-depositional modifications. *Mineralium Deposita*, *51*(6), 797–822. https://doi.org/10.1007/s00126-015-0631-y

Israel, C., Boyet, M., Doucelance, R., Bonnand, P., Frossard, P., Auclair, D., & Bouvier, A. (2020). Formation of the Ce-Nd mantle array: Crustal extraction vs. recycling by subduction. *Earth and Planetary Science Letters*, *530*, 115941. https://doi.org/10.1016/j.epsl.2019.115941

Ji, X.-X., Zhou, S., Chen, Q., Liu, D.-M., & Li, D.-W. (2016). Provenance and tectonic setting of the Kunyang Group in central Yunnan Province. *Geology in China*, *43*(3), 857–878. https://doi.org/10.12029/gc20160312

Kato, Y., Fujinaga, K., Nakamura, K., Takaya, Y., Kitamura, K., Ohta, J., et al. (2011). Deep-sea mud in the Pacific Ocean as a potential resource for rare-earth elements. *Nature Geoscience*, *4*(8), 535–539. https://doi.org/10.1038/ngeo1185

Krupenin, M. T., Kuznetsov, A. B., Zamyatin, D. A., Pankrushina, E. A., & Lepekha, S. V. (2023). Composition and formation conditions of Neoproterozoic phosphorites in the Middle Urals. *Lithology and Mineral Resources*, *58*(2), 95–121. https://doi.org/10.1134/s0024490222700067

Li, J., Shi, X., Huang, M., Yu, M., Bi, D., Song, Z., et al. (2023). The transformation and accumulation mechanism of rare earth elements in deep-sea sediments from the Wharton Basin, Indian Ocean. *Ore Geology Reviews*, *161*, 105655. https://doi.org/10.1016/j.oregeorev.2023.105655

Li, N.-B., Niu, H.-C., Shan, Q., & Weng, Q. (2022). Subducted sediment contributions to REE deposits recorded by alkaline mafic dikes in the Lizhuang REE deposit, Panxi area, southwest China. *Ore Geology Reviews*, *140*, 104567. https://doi.org/10.1016/j.oregeorev.2021.104567

Li, W., Nakada, R., Takahashi, Y., Gaschnig, R. M., Hu, Y., Shakouri, M., et al. (2023). Cerium geochemical composition of the upper continental crust through time: Implications for tracing past surface redox conditions. *Geochimica et Cosmochimica Acta*, *359*, 20–29. https://doi.org/10.1016/j.gca.2023.08.024

Li, X.-C., Fan, H.-R., Su, J.-H., Groves, D. I., Yang, K.-F., & Zhao, X.-F. (2024). Giant REE accumulation related to voluminous, highly evolved carbonatite: A microanalytical study of carbonate minerals from the Bayan Obo deposit, China. *Economic Geology*, *119*(2), 373–393. https://doi.org/10.5382/econgeo.5060

Li, X.-C., Zhou, M.-F., Li, S.-H., Zhang, X.-R., Fan, H.-R., Groves, D. I., & Xuan Dac, N. (2023). An unusual early Eocene, syncollisional carbonatite complex and related rare earth element deposit in the India-Asia collision zone, northwestern Vietnam. *Economic Geology*, *118*(1), 237–256. https://doi.org/10.5382/econgeo.4969

Liao, J., Chen, J., Sun, X., Deng, Y., Wang, Y., Wang, D., et al. (2024). Controlling factors on REY enrichments in basins from the Pacific Ocean: Early diagenesis and local constraints. *Geochemistry, Geophysics, Geosystems*, *25*(1), e2023GC011111. https://doi.org/10.1029/2023gc011111

Liu, H., Zi, J.-W., Cawood, P. A., Cui, X., & Zhang, L. (2020). Reconstructing South China in the Mesoproterozoic and its role in the Nuna and Rodinia supercontinents. *Precambrian Research*, *337*, 105558. https://doi.org/10.1016/j.precamres.2019.105558

Liu, X. M., Kah, L. C., Knoll, A. H., Cui, H., Wang, C., Bekker, A., & Hazen, R. M. (2021). A persistently low level of atmospheric oxygen in Earth's middle age. *Nature Communications*, *12*(1), 351. https://doi.org/10.1038/s41467-020-20484-7

Mazumdar, A., Tanaka, K., Takahashi, T., & Kawabe, I. (2003). Characteristics of rare earth element abundances in shallow marine continental platform carbonates of Late Neoproterozoic successions from India. *Geochemical Journal*, *37*(2), 277–289. https://doi.org/10.2343/geochemj.37.277

McCoy-West, A. J., Bennett, V. C., & Amelin, Y. (2016). Rapid Cenozoic ingrowth of isotopic signatures simulating "HIMU" in ancient lithospheric mantle: Distinguishing source from process. *Geochimica et Cosmochimica Acta*, *187*, 79–101. https://doi.org/10.1016/j.gca.2016.05.013

Menendez, A., James, R. H., Roberts, S., Peel, K., & Connelly, D. (2017). Controls on the distribution of rare earth elements in deep-sea sediments in the North Atlantic Ocean. *Ore Geology Reviews*, *87*, 100–113. https://doi.org/10.1016/j.oregeorev.2016.09.036

Mimura, K., Nakamura, K., Yasukawa, K., Machida, S., Ohta, J., Fujinaga, K., & Kato, Y. (2019). Significant impacts of pelagic clay on average chemical composition of subducting sediments: New insights from discovery of extremely rare-earth elements and yttrium-rich mud at Ocean Drilling Program Site 1149 in the western North Pacific Ocean. *Journal of Asian Earth Sciences*, *186*, 104059. https://doi.org/10.1016/j.jseaes.2019.104059

Moore, M., Chakhmouradian, A. R., Mariano, A. N., & Sidhu, R. (2015). Evolution of rare-earth mineralization in the Bear Lodge carbonatite, Wyoming: Mineralogical and isotopic evidence. *Ore Geology Reviews*, *64*, 499–521. https://doi.org/10.1016/j.oregeorev.2014.03.015

Nabyl, Z., Gaillard, F., Tuduri, J., & Carlo, I. D. (2021). No direct effect of F, Cl and P on REE partitioning between carbonate and alkaline silicate melts. *Comptes Rendus Geoscience*, *353*(S2), 233–272. https://doi.org/10.5802/crgeos.104

Nabyl, Z., Massuyeau, M., Gaillard, F., Tuduri, J., Iacono-Marziano, G., Rogerie, G., et al. (2020). A window in the course of alkaline magma differentiation conducive to immiscible REE-rich carbonatites. *Geochimica et Cosmochimica Acta*, *282*, 297–323. https://doi.org/10.1016/j.gca.2020.04.008

Nagender, N. B., Bau, M., Ramalingeswara, R. B., & Rao, C. M. (1997). Trace and rare earth elemental variation in Arabian Sea sediments through a transect across the oxygen minimum zone. *Geochimica et Cosmochimica Acta*, *61*(12), 2375–2388. https://doi.org/10.1016/s0016-7037(97)00094-x

Nedosekova, I., Vladykin, N., Udoratina, O., & Belyatsky, B. (2021). Ore and geochemical specialization and substance sources of the Ural and Timan carbonatite complexes (Russia): Insights from trace element, Rb–Sr, and Sm–Nd isotope data. *Minerals*, *11*(7), 711. https://doi.org/10.3390/min11070711

Nelson, D. R., Chivas, A. R., Chappell, B. W., & McCulloch, M. T. (1988). Geochemical and isotopic systematics in carbonatites and implications for the evolution of ocean-island sources. *Geochimica et Cosmochimica Acta*, *52*(1), 1–17. https://doi.org/10.1016/0016-7037(88)90051-8

O'Neill, H. S. C. (2016). The smoothness and shapes of chondrite-normalized rare earth element patterns in basalts. *Journal of Petrology*, *57*(8), 1463–1508. https://doi.org/10.1093/petrology/egw047

Palme, H., & O'Neill, H. S. C. (2014). Cosmochemical estimates of mantle composition. In R. W. Carlson (Ed.), *Treatise on geochemistry*, *The mantle and Core* (2nd ed., Vol. 3, pp. 1–39). Elsevier. https://doi.org/10.1016/b978-0-08-095975-7.00201-1

Patel, A. K., Mishra, B., Upadhyay, D., & Pruseth, K. L. (2022). Mineralogical and geochemical evidence of dissolution-reprecipitation controlled hydrothermal rare earth element mineralization in the Amba Dongar carbonatite complex, Gujarat, Western India. *Economic Geology*, *117*(3), 683–702. https://doi.org/10.5382/econgeo.4890

Pattan, J. N., & Higgs, N. C. (1995). Rare earth element studies of surficial sediments from the southwestern Carlsberg Ridge, Indian Ocean. *Journal of Earth System Science*, *104*(4), 569–578. https://doi.org/10.1007/bf02839297

Pintér, Z., Foley, S. F., Yaxley, G. M., Rosenthal, A., Rapp, R. P., Lanati, A. W., & Rushmer, T. (2021). Experimental investigation of the composition of incipient melts in upper mantle peridotites in the presence of CO_2 and H_2O. *Lithos*, *396–397*, 106224. https://doi.org/10.1016/j.lithos.2021.106224

Plank, T. (2014). The chemical composition of subducting sediments. In *Treatise on geochemistry*. In *The crust* (2nd ed., Vol. 4, pp. 607–629). Elsevier. https://doi.org/10.1016/b978-0-08-095975-7.00319-3

Plank, T., & Langmuir, C. H. (1998). The chemical composition of subducting sediment and its consequences for the crust and mantle. *Chemical Geology*, *145*(3–4), 325–394. https://doi.org/10.1016/s0009-2541(97)00150-2

Rao, V. P., Hegner, E., Naqvi, S. W. A., Kessarkar, P. M., Ahmad, S. M., & Raju, D. S. (2008). Miocene phosphorites from the Murray Ridge, northwestern Arabian Sea. *Palaeogeography, Palaeoclimatology, Palaeoecology*, *260*(3–4), 347–358. https://doi.org/10.1016/j.palaeo.2007.12.003

R Core Team. (2023). R: A language and environment for statistical computing [Software]. *Vienna, Austria: R Foundation for Statistical Computing*. Retrived from https://www.r-project.org/

Ren, J., He, G., Yao, H., Deng, X., Zhu, K., & Yang, S. (2017). The effects of phosphatization on the REY of Co-rich Fe-Mn crusts. *Marine Geology and Quaternary Geology*, *37*(2), 33–43. https://doi.org/10.16562/j.cnki.0256-1492.2017.02.004

Ren, J., He, G., Zhu, K., Deng, X., Liu, J., Fu, P., et al. (2017). REY-rich phosphate and its effects on the deep-sea mud mineralization. *Acta Geologica Sinica*, *91*(6), 1312–1325. https://www.geojournals.cn/dzxb/dzxb/article/abstract/2017060004

Ren, J., Jiang, X., He, G., Wang, F., Yang, T., Luo, S., et al. (2022). Enrichment and sources of REY in phosphate fractions: Constraints from the leaching of REY-rich deep-sea sediments. *Geochimica et Cosmochimica Acta*, *335*, 155–168. https://doi.org/10.1016/j.gca.2022.08.035

Ren, J., Liu, Y., Wang, F., He, G., Deng, X., Wei, Z., & Yao, H. (2021). Mechanism and influencing factors of REY enrichment in deep-sea sediments. *Minerals*, *11*(2), 196. https://doi.org/10.3390/min11020196

Ren, J., Yao, H., Zhu, K., He, G., Deng, X., Wang, H., et al. (2015). Enrichment mechanism of rare earth elements and yttrium in deep-sea mud of Clarion-Clipperton Region. *Earth Science Frontiers*, *22*(4), 200–211. https://doi.org/10.13745/j.esf.2015.04.021

Schlüter, J., Malcherek, T., Husdal, T. A., & Andersen (2009). The new mineral stetindite, $CeSiO_4$, a cerium end-member of the zircon group. *Neues Jahrbuch für Mineralogie - Abhandlungen*, *186*(2), 195–200. https://doi.org/10.1127/0077-7757/2009/0146

Shields, G., & Stille, P. (1998). Stratigraphic trends in cerium anomaly in authigenic marine carbonates and phosphates: Diagenetic alteration or seawater signals? *Mineralogical Magazine, Mineralogical Magazine, Goldschmidt Conference, Toulouse, France*, *62A*(3), 1387–1388. https://doi.org/10.1180/minmag.1998.62a.3.60

Simandl, G. J., & Paradis, S. (2018). Carbonatites: Related ore deposits, resources, footprint, and exploration methods. *Applied Earth Science*, *127*(4), 123–152. https://doi.org/10.1080/25726838.2018.1516935

Simonetti, A., & Bell, K. (1994). Isotopic and geochemical investigation of the Chilwa Island carbonatite complex, Malawi: Evidence for a depleted mantle source region, liquid immiscibility, and open-system behaviour. *Journal of Petrology*, *35*(6), 1597–1621. https://doi.org/10.1093/petrology/35.6.1597

Sirocko, F. (2000). Processes controlling trace element geochemistry of Arabian Sea sediments during the last 25,000 years. *Global and Planetary Change*, *26*(1–3), 217–303. https://doi.org/10.1016/s0921-8181(00)00046-1

Slezak, P., & Spandler, C. (2019). Carbonatites as recorders of mantle-derived magmatism and subsequent tectonic events: An example of the Gifford Creek Carbonatite Complex, Western Australia. *Lithos*, *328–329*, 212–227. https://doi.org/10.1016/j.lithos.2019.01.028

Smith, M. P., Moore, K., Kavecsánszki, D., Finch, A. A., Kynicky, J., & Wall, F. (2016). From mantle to critical zone: A review of large and giant sized deposits of the rare earth elements. *Geoscience Frontiers*, *7*(3), 315–334. https://doi.org/10.1016/j.gsf.2015.12.006

Song, W., Xu, C., Smith, M. P., Kynicky, J., Yang, J., Liu, T., & Jing, D. (2023). Origin of heavy rare earth element enrichment in carbonatites. *Geochimica et Cosmochimica Acta*, *362*, 115–126. https://doi.org/10.1016/j.gca.2023.08.025

Spandler, C., Slezak, P., & Nazari-Dehkordi, T. (2020). Tectonic significance of Australian rare earth element deposits. *Earth-Science Reviews*, *207*, 103219. https://doi.org/10.1016/j.earscirev.2020.103219

Sun, J., Zhu, X. K., Belshaw, N. S., Chen, W., Doroshkevich, A. G., Luo, W. J., et al. (2021). Ca isotope systematics of carbonatites: Insights into carbonatite source and evolution. *Geochemical Perspectives Letters*, *17*, 11–15. https://doi.org/10.7185/geochemlet.2107

Takaya, Y., Yasukawa, K., Kawasaki, T., Fujinaga, K., Ohta, J., Usui, Y., et al. (2018). The tremendous potential of deep-sea mud as a source of rare-earth elements. *Scientific Reports*, *8*(1), 5763. https://doi.org/10.1038/s41598-018-23948-5

Tanaka, E., Nakamura, K., Yasukawa, K., Mimura, K., Fujinaga, K., Iijima, K., et al. (2020). Chemostratigraphy of deep-sea sediments in the western North Pacific Ocean: Implications for genesis of mud highly enriched in rare-earth elements and yttrium. *Ore Geology Reviews*, *119*, 103392. https://doi.org/10.1016/j.oregeorev.2020.103392

Tang, D., Shi, X., Wang, X., & Jiang, G. (2016). Extremely low oxygen concentration in mid-Proterozoic shallow seawaters. *Precambrian Research*, *276*, 145–157. https://doi.org/10.1016/j.precamres.2016.02.005

Tassara, S., Gonzalez-Jimenez, J. M., Reich, M., Schilling, M. E., Morata, D., Begg, G., et al. (2017). Plume-subduction interaction forms large auriferous provinces. *Nature Communications*, *8*(1), 843. https://doi.org/10.1038/s41467-017-00821-z

Thomsen, T. B., & Schmidt, M. W. (2008). Melting of carbonated pelites at 2.5–5.0 GPa, silicate–carbonatite liquid immiscibility, and potassium–carbon metasomatism of the mantle. *Earth and Planetary Science Letters*, *267*(1–2), 17–31. https://doi.org/10.1016/j.epsl.2007.11.027

Tsuno, K., Dasgupta, R., Danielson, L., & Righter, K. (2012). Flux of carbonate melt from deeply subducted pelitic sediments: Geophysical and geochemical implications for the source of Central American volcanic arc. *Geophysical Research Letters*, *39*(16), L16307. https://doi.org/10.1029/2012gl052606

Tucker, R. D., Belkin, H. E., Schulz, K. J., Peters, S. G., Horton, F., Buttleman, K., & Scott, E. R. (2012). A major light rare-earth element (LREE) resource in the Khanneshin Carbonatite Complex, Southern Afghanistan. *Economic Geology*, *107*(2), 197–208. https://doi.org/10.2113/econgeo.107.2.197

van der Meer, Q. H. A., Waight, T. E., Scott, J. M., & Münker, C. (2017). Variable sources for Cretaceous to recent HIMU and HIMU-like intraplate magmatism in New Zealand. *Earth and Planetary Science Letters*, *469*, 27–41. https://doi.org/10.1016/j.epsl.2017.03.037

Vasyukova, O. V., & Williams-Jones, A. E. (2022). Carbonatite metasomatism, the key to unlocking the carbonatite-phoscorite-ultramafic rock paradox. *Chemical Geology*, *602*, 120888. https://doi.org/10.1016/j.chemgeo.2022.120888

Viladkar, S. G., & Sorokhtina, N. V. (2021). Evolution of pyrochlore in carbonatites of the Amba Dongar complex, India. *Mineralogical Magazine*, *85*(4), 554–567. https://doi.org/10.1180/mgm.2021.50

Walter, B. F., Giebel, R. J., Steele-MacInnis, M., Marks, M. A. W., Kolb, J., & Markl, G. (2021). Fluids associated with carbonatitic magmatism: A critical review and implications for carbonatite magma ascent. *Earth-Science Reviews*, *215*, 103509. https://doi.org/10.1016/j.earscirev.2021.103509

Wang, F., He, G., Deng, X., Yang, Y., & Ren, J. (2021). Fish teeth Sr isotope stratigraphy and Nd isotope variations: New insights on REY enrichments in deep-sea sediments in the Pacific. *Journal of Marine Science and Engineering*, *9*(12), 1379. https://doi.org/10.3390/jmse9121379

Wang, F., He, G., Yao, H., & Deng, X. (2017). The progress in the study of REE-rich deep-sea sediments. *Geology in China*, *44*(3), 449–459. https://doi.org/10.12029/gc20170304

Weng, Q., Yang, W.-B., Niu, H.-C., Li, N.-B., Qu, P., Shan, Q., et al. (2021). B–Sr–Nd–Pb isotopic constraints on the origin of the Maoniuping alkaline syenite–carbonatite complex, SW China. *Ore Geology Reviews*, *135*, 104193. https://doi.org/10.1016/j.oregeorev.2021.104193

White, W. M. (2015). Probing the Earth's deep interior through geochemistry. *Geochemical Perspectives*, *4*(2), 95–251. https://doi.org/10.7185/geochempersp.4.2

Xin, H., Jiang, S., Yang, J., Wu, H., & Pi, D. (2016). Rare earth element geochemistry of phosphatic rocks in Neoproterozoic Ediacaran Doushantuo Formation in Hushan Section from the Yangtze Gorges Area, South China. *Journal of Earth Science*, *27*(2), 204–210. https://doi.org/10.1007/s12583-015-0653-5

Xin, H., Jiang, S.-Y., Yang, J.-H., Wu, H.-P., & Pi, D.-H. (2015). Rare Earth element and Sr–Nd isotope geochemistry of phosphatic rocks in Neoproterozoic Ediacaran Doushantuo Formation in Zhangcunping section from western Hubei Province, South China. *Palaeogeography, Palaeoclimatology, Palaeoecology*, *440*, 712–724. https://doi.org/10.1016/j.palaeo.2015.09.034

Xue, S., Ling, M.-X., Liu, Y.-L., & Sun, W. (2018). Recycling of subducted carbonates: Formation of the Taohuala Mountain carbonatite, North China Craton. *Chemical Geology*, *478*, 89–101. https://doi.org/10.1016/j.chemgeo.2017.10.039

Yang, K., Fan, H., Pirajno, F., & Li, X. (2019). The Bayan Obo (China) giant REE accumulation conundrum elucidated by intense magmatic differentiation of carbonatite. *Geology*, *47*(12), 1198–1202. https://doi.org/10.1130/g46674.1

Yang, L.-Q., Deng, J., Groves, D. I., Santosh, M., He, W.-Y., Li, N., et al. (2022). Metallogenic "factories" and resultant highly anomalous mineral endowment on the craton margins of China. *Geoscience Frontiers*, *13*(2), 101339. https://doi.org/10.1016/j.gsf.2021.101339

Yang, Y. (2003). *Study on geochemistry of Fe-Cu-REE deposit in Kunyang group in Mid-Proterozoic-exampled by the Yinachang Fe-Cu-REE deposit* PhD thesis. The Key lab of ore Geochemistry, Chinese Academy of Science, Guiyang.

Yasukawa, K., Kino, S., Azami, K., Tanaka, E., Mimura, K., Ohta, J., et al. (2020). Geochemical features of Fe-Mn micronodules in deep-sea sediments of the western North Pacific Ocean: Potential for co-product metal extraction from REY-rich mud. *Ore Geology Reviews*, *127*, 103805. https://doi.org/10.1016/j.oregeorev.2020.103805

Yasukawa, K., Liu, H., Fujinaga, K., Machida, S., Haraguchi, S., Ishii, T., et al. (2014). Geochemistry and mineralogy of REY-rich mud in the eastern Indian Ocean. *Journal of Asian Earth Sciences*, *93*, 25–36. https://doi.org/10.1016/j.jseaes.2014.07.005

Yasukawa, K., Nakamura, K., Fujinaga, K., Iwamori, H., & Kato, Y. (2016). Tracking the spatiotemporal variations of statistically independent components involving enrichment of rare-earth elements in deep-sea sediments. *Scientific Reports*, *6*(1), 29603. https://doi.org/10.1038/srep29603

Yaxley, G. M., Anenburg, M., Tappe, S., Decree, S., & Guzmics, T. (2022). Carbonatites: Classification, sources, evolution, and emplacement. *Annual Review of Earth and Planetary Sciences*, *50*(1), 261–293. https://doi.org/10.1146/annurev-earth-032320-104243

Yaxley, G. M., Kjarsgaard, B. A., & Jaques, A. L. (2021). Evolution of carbonatite magmas in the upper mantle and crust. *Elements*, *17*(5), 315–320. https://doi.org/10.2138/gselements.17.5.315

Yu, M., Shi, X., Huang, M., Liu, J., Yan, Q., Yang, G., et al. (2021). The transfer of rare earth elements during early diagenesis in REY-rich sediments: An example from the Central Indian Ocean Basin. *Ore Geology Reviews*, *136*, 104269. https://doi.org/10.1016/j.oregeorev.2021.104269

Zhang, H., Zhou, J., Yuan, P., Dong, Y., Fan, W., Chu, F., et al. (2023). Highly positive Ce anomalies of hydrogenetic ferromanganese micronodules from abyssal basins in the NW and NE Pacific: Implications for REY migration and enrichment in deep-sea sediments. *Ore Geology Reviews*, *154*, 105324. https://doi.org/10.1016/j.oregeorev.2023.105324

Zhang, K., & Shields, G. A. (2022). Sedimentary Ce anomalies: Secular change and implications for paleoenvironmental evolution. *Earth-Science Reviews*, *229*, 104015. https://doi.org/10.1016/j.earscirev.2022.104015

Zhang, X., Tao, C., Shi, X., Li, H., Huang, M. U., & Huang, D. (2017). Geochemical characteristics of REY-rich pelagic sediments from the GC02 in central Indian Ocean Basin. *Journal of Rare Earths*, *35*(10), 1047–1058. https://doi.org/10.1016/s1002-0721(17)61012-3

Zhang, X. Y., Chen, L. H., Wang, X. J., Hanyu, T., Hofmann, A. W., Komiya, T., et al. (2022). Zinc isotopic evidence for recycled carbonate in the deep mantle. *Nature Communications*, *13*(1), 6085. https://doi.org/10.1038/s41467-022-33789-6

Zhao, X.-C., Yan, S., Niu, H.-C., Zhang, Q.-B., Zhao, X., Wu, J., & Yang, W.-B. (2021). Isotopic fingerprints of recycled eclogite facies sediments in the generation of the Huanglongpu carbonatite, central China. *Ore Geology Reviews*, *139*, 104534. https://doi.org/10.1016/j.oregeorev.2021.104534

Zheng, X., Liu, Y., Smith, M. P., Kynický, J., & Hou, Z. (2023). Carbonatitic magma fractionation and contamination generate rare earth element enrichment and mineralization in the Maoniuping giant REE deposit, SW China. *Journal of Petrology*, *64*(6), egad037. https://doi.org/10.1093/petrology/egad037

Zhu, X., Liu, Y., & Hou, Z. (2024). Massive rare earth element storage in sub-continental lithospheric mantle initiated by diapirism, not by melting. *Geology*, *52*(2), 105–109. https://doi.org/10.1130/g51102.1